

Dear Author,

Here are the proofs of your article.

- You can submit your corrections **online**, via **e-mail** or by **fax**.
- For **online** submission please insert your corrections in the online correction form. Always indicate the line number to which the correction refers.
- You can also insert your corrections in the proof PDF and **email** the annotated PDF.
- For fax submission, please ensure that your corrections are clearly legible. Use a fine black pen and write the correction in the margin, not too close to the edge of the page.
- Remember to note the **journal title, article number, and your name** when sending your response via e-mail or fax.
- **Check** the metadata sheet to make sure that the header information, especially author names and the corresponding affiliations are correctly shown.
- **Check** the questions that may have arisen during copy editing and insert your answers/ corrections.
- **Check** that the text is complete and that all figures, tables and their legends are included. Also check the accuracy of special characters, equations, and electronic supplementary material if applicable. If necessary refer to the *Edited manuscript*.
- The publication of inaccurate data such as dosages and units can have serious consequences. Please take particular care that all such details are correct.
- Please **do not** make changes that involve only matters of style. We have generally introduced forms that follow the journal's style. Substantial changes in content, e.g., new results, corrected values, title and authorship are not allowed without the approval of the responsible editor. In such a case, please contact the Editorial Office and return his/her consent together with the proof.
- If we do not receive your corrections **within 48 hours**, we will send you a reminder.
- Your article will be published **Online First** approximately one week after receipt of your corrected proofs. This is the **official first publication** citable with the DOI. **Further changes are, therefore, not possible.**
- The **printed version** will follow in a forthcoming issue.

Please note

After online publication, subscribers (personal/institutional) to this journal will have access to the complete article via the DOI using the URL: [http://dx.doi.org/\[DOI\]](http://dx.doi.org/[DOI]).

If you would like to know when your article has been published online, take advantage of our free alert service. For registration and further information go to: <http://www.link.springer.com>.

Due to the electronic nature of the procedure, the manuscript and the original figures will only be returned to you on special request. When you return your corrections, please inform us if you would like to have these documents returned.

Metadata of the article that will be visualized in OnlineFirst

ArticleTitle	Kinetic relations and local energy balance for LEFM from a nonlocal peridynamic model	
Article Sub-Title		
Article CopyRight	Springer Nature B.V. (This will be the copyright line in the final PDF)	
Journal Name	International Journal of Fracture	
Corresponding Author	Family Name	Lipton
	Particle	
	Given Name	Robert P.
	Suffix	
	Division	Department of Mathematics and Center for Computation and Technology
	Organization	Louisiana State University
	Address	Baton Rouge, LA, 70803, USA
	Phone	
	Fax	
	Email	lipton@lsu.edu
	URL	
	ORCID	http://orcid.org/0000-0002-1382-3204
Author	Family Name	Jha
	Particle	
	Given Name	Prashant K.
	Suffix	
	Division	Oden Institute for Computational Engineering and Sciences
	Organization	The University of Texas at Austin
	Address	Austin, TX, 78712, USA
	Phone	
	Fax	
	Email	pjha@utexas.edu
	URL	
	ORCID	http://orcid.org/0000-0003-2158-364X
Schedule	Received	23 March 2020
	Revised	
	Accepted	24 August 2020
Abstract	A simple nonlocal field theory of peridynamic type is applied to model brittle fracture. The kinetic relation for the crack tip velocity given by Linear Elastic Fracture Mechanics (LEFM) is recovered directly from the nonlocal dynamics, this is seen both theoretically and in simulations. An explicit formula for the change of internal energy inside a neighborhood enclosing the crack tip is found for the nonlocal model and applied to LEFM.	
Keywords (separated by '-')	Fracture - Peridynamics - LEFM - Fracture toughness - Stress intensity - Local power balance	
Footnote Information	This material is based upon work supported by the U. S. Army Research Laboratory and the U. S. Army Research Office under contract/grant number W911NF1610456.	



Kinetic relations and local energy balance for LEFM from a nonlocal peridynamic model

Prashant K. Jha · Robert P. Lipton

Received: 23 March 2020 / Accepted: 24 August 2020
© Springer Nature B.V. 2020

Abstract A simple nonlocal field theory of peridynamic type is applied to model brittle fracture. The kinetic relation for the crack tip velocity given by Linear Elastic Fracture Mechanics (LEFM) is recovered directly from the nonlocal dynamics, this is seen both theoretically and in simulations. An explicit formula for the change of internal energy inside a neighborhood enclosing the crack tip is found for the nonlocal model and applied to LEFM.

Keywords Fracture · Peridynamics · LEFM · Fracture toughness · Stress intensity · Local power balance

1 Introduction

The fracture of solids can be viewed as a collective interaction across length scales. Application of sufficient stress or strain to a brittle material breaks atomistic bonds leading to fracture at macroscopic scales.

This material is based upon work supported by the U. S. Army Research Laboratory and the U. S. Army Research Office under contract/grant number W911NF1610456.

P. K. Jha
Oden Institute for Computational Engineering and Sciences, The University of Texas at Austin, Austin, TX 78712, USA e-mail: pjha@utexas.edu

R. P. Lipton (✉)
Department of Mathematics and Center for Computation and Technology, Louisiana State University, Baton Rouge, LA 70803, USA e-mail: lipton@lsu.edu

The appeal of a nonlocal fracture theory like peridynamics Silling (2000), Silling et al. (2007) is that fracture is captured as an emergent phenomenon. At the same time such a theory needs to recover the established theory of dynamic fracture mechanics described in Freund (1990), Ravi-Chandar (2004), Anderson (2005), Slepian (2002) as a limiting case. Motivated by these observations we consider a nonlocal peridynamic model (cohesive dynamics) proposed in Lipton (2014, 2016). The length scale of nonlocal interaction between any material point and its neighbors is called the *horizon*. Here the force strain relation between two points is linear elastic for small strains, softens under sufficiently large strain and ultimately becomes zero, see Fig. 2. In this nonlocal model displacement gradients can become steep and localize onto thin regions, see Jha and Lipton (2020). This model is used to show the kinetic relation for the velocity of the crack tip given by LEFM Freund (1990) follows in the limit of vanishing horizon.

In this paper the kinetic relation of LEFM is recovered from the nonlocal model in two different ways. The first approach to recovering the kinetic relation is to note that the same equation of motion applies everywhere in the body for the nonlocal model. We use this to show that local power balance is given by the stationarity in time of the internal energy of a small domain containing the crack tip. The change in internal energy is shown to be the difference between the elastic energy flowing into the crack and the kinetic energy

Author Proof

I

47 and stress work flux flowing into the domain, which is
 48 given by formula (18). To leading order the stress work
 49 flux is precisely the rate of energy needed to create
 50 new surface (21). These results are obtained directly
 51 and exclusively from the dynamics governed by the
 52 nonlocal Cauchy equations of motion for a continuum
 53 body. This is the explicit connection between the non-
 54 local Cauchy equations of motion derived from double
 55 well potentials and the energy rate required to make
 56 new surface. For remote boundary loading we apply
 57 energy balance and pass to the local limit to recover
 58 the celebrated kinetic relation for the modern theo-
 59 ry of dynamic fracture mechanics articulated in Fre-
 60 und (1990), Ravi-Chandar (2004), Anderson (2005),
 61 Slepian (2002), see 4.1. Next it is shown that local
 62 power balance must hold for the nonlocal model when
 63 the displacement field is translation invariant inside a
 64 neighborhood of the crack (see Sect. 4.2). We pass to
 65 the limit of vanishing horizon to recover that the same
 66 holds true for LEFM. As a second approach we develop
 67 a nonlocal dynamic J integral and apply Mott's hypothe-
 68 sis on energy balance to a small region surrounding
 69 the crack tip. This is done in Sect. 4.3. The kinetic
 70 relation of LFEM is then obtained from the nonlocal
 71 model by passing the limit of vanishing nonlocality.
 72 Here it is pointed out that the approach of Sect. 4.1 is
 73 self contained and follows exclusively from the nonlo-
 74 cal Cauchy equation of motion. On the other hand the
 75 approach of Sect. 4.3 follows the classic one Freund
 76 (1990) and uses the nonlocal model to only compute
 77 the flow of elastic energy into the crack tip.

78 Next we provide a computational example to illus-
 79 trate that power balance holds in the neighborhood of
 80 the crack tip using the nonlocal model. The fracture
 81 toughness \mathcal{G}_c , density, and elastic modulus of the mate-
 82 rial are prescribed. The numerical simulation using the
 83 nonlocal model is carried out for a single edge notch
 84 specimen of finite width and length. The simulation
 85 delivers a mode I crack traveling with constant veloc-
 86 ity at roughly half of the Rayleigh wave speed. This
 87 simulation is consistent with the experimental results
 88 reported in Goldman et al. (2010). The change in inter-
 89 nal energy inside a small neighborhood is calculated
 90 using (18) and is zero, i.e., power balance holds for
 91 a dynamic crack traveling at constant velocity V . The
 92 elastic energy flowing into a small neighborhood of the
 93 crack tip is \mathcal{F} and the power balance inside a neighbor-

hood of diameter δ is of the form

$$\mathcal{G}_c \approx \frac{\mathcal{F}}{V}. \quad (1)$$

Here \approx indicates agreement to leading order in δ .
 This demonstrates that the energy released per unit
 length during crack growth at constant velocity is equal
 to the elastic energy flowing into the crack tip (see
 Sect. 5). It is important to note that the power balance
 (1) emerges through simulation and calculation using
 (18) as opposed to being independently postulated on
 physical grounds. In other words local power balance
 is a consequence of the nonlocal dynamics. The simu-
 lation and calculation are described in Sect. 5.

The paper is organized as follows: The nonlocal
 model of peridynamic type is presented in Sect. 2.
 Sect. 3 describes the fracture toughness and elastic
 properties associated with the nonlocal model. The
 main results given by the local energy balance and the
 recovery of the kinetic relation for LEFM are presented
 in 4. For clarity that we postpone the derivations - cal-
 culations for later (see Sects. 6 and 7) and present
 simulations that emphasize the local energy balance in
 Sect. 5. Section 6 calculates the energy flow into the
 crack tip for the nonlocal model. Section 7 explicitly
 shows how the stress work flowing into the crack tip
 corresponds to the power required to create new frac-
 ture surface. The results are summarized in Sect. 8.

2 Nonlocal modeling

The appeal of nonlocal peridynamic models is that frac-
 ture appears as an emergent phenomena generated by
 the underlying field theory eliminating the need for
 supplemental kinetic relations describing crack growth.
 The deformation field inside the body for points \mathbf{x}
 at time t is written $\mathbf{u}(\mathbf{x}, t)$. The peridynamic model is
 described simply by the balance of linear momentum
 of the form

$$\rho \mathbf{u}_{tt}(\mathbf{x}, t) = \int_{\mathcal{H}_\epsilon(\mathbf{x})} \mathbf{f}(\mathbf{y}, \mathbf{x}) d\mathbf{y} + \mathbf{b}(\mathbf{x}, t) \quad (2)$$

where $\mathcal{H}_\epsilon(\mathbf{x})$ is a neighborhood of \mathbf{x} , ρ is the density,
 \mathbf{b} is the body force density field, and \mathbf{f} is a material-
 dependent constitutive law that represents the force
 density that a point \mathbf{y} inside the neighborhood exerts
 on \mathbf{x} as a result of the deformation field. The radius ϵ
 of the neighborhood is referred to as the *horizon*. Here
 all points satisfy the same basic field equations (2).

Fig. 1 Single-edge-notch

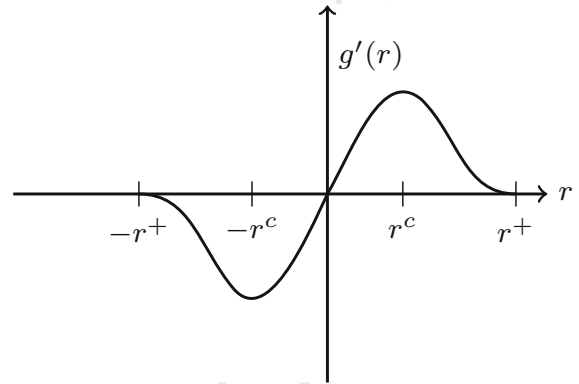
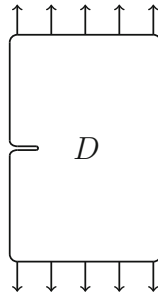


Fig. 2 Cohesive force. The force goes smoothly to zero at $\pm r^+$

This approach to fracture modeling was introduced in Silling (2000) and Silling et al. (2007).

We work with a class of peridynamic models with nonlocal forces derived from double well potentials. See Lipton (2014), Lipton (2016). The term double well describes the force potential between two points. One of the wells is degenerate and appears at infinity while the other is at zero strain. For small strains the nonlocal force is linearly elastic but for larger strains the force begins to soften and then approaches zero after reaching a critical strain. The associated nonlocal dynamics is called *cohesive dynamics*. We consider a single edge notch specimen as given in Fig. 1 in plane stress.

In this treatment the displacement field $\mathbf{u} : D \times [0, T] \rightarrow \mathbb{R}^2$ is small compared to the size of the specimen D and the deformed configuration is the same as the reference configuration. We have $\mathbf{u} = \mathbf{u}(\mathbf{x}, t)$ as a function of space and time but will suppress the \mathbf{x} dependence when convenient and write $\mathbf{u}(t)$. The tensile strain S between two points \mathbf{x}, \mathbf{y} in D along the direction $\mathbf{e}_{\mathbf{y}-\mathbf{x}}$ is defined as

$$S(\mathbf{y}, \mathbf{x}, \mathbf{u}(t)) = \frac{\mathbf{u}(\mathbf{y}, t) - \mathbf{u}(\mathbf{x}, t)}{|\mathbf{y} - \mathbf{x}|} \cdot \mathbf{e}_{\mathbf{y}-\mathbf{x}}, \quad (3)$$

where $\mathbf{e}_{\mathbf{y}-\mathbf{x}} = \frac{\mathbf{y}-\mathbf{x}}{|\mathbf{y}-\mathbf{x}|}$ is a unit vector and “ \cdot ” is the dot product.

In the double well model the force acting between material points \mathbf{x} and \mathbf{y} is initially elastic and then softens and decays to zero as the strain between points increases, see Fig. 2. The critical strain $S_c > 0$ for which the force begins to soften is given by

$$S_c = \frac{r^c}{\sqrt{|\mathbf{y} - \mathbf{x}|}}, \quad (4)$$

and S_+ is the strain at which the force goes to zero

$$S_+ = \frac{r^+}{\sqrt{|\mathbf{y} - \mathbf{x}|}}. \quad (5)$$

The nonlocal force is defined in terms of a double well potential. The potential is a function of the strain and is defined for all \mathbf{x}, \mathbf{y} in D by

$$\mathcal{W}^\epsilon(S(\mathbf{y}, \mathbf{x}, \mathbf{u}(t))) = J^\epsilon(|\mathbf{y} - \mathbf{x}|) \frac{1}{\epsilon^3 \omega_2 |\mathbf{y} - \mathbf{x}|} g(\sqrt{|\mathbf{y} - \mathbf{x}|} S(\mathbf{y}, \mathbf{x}, \mathbf{u}(t))) \quad (6)$$

where $\mathcal{W}^\epsilon(S(\mathbf{y}, \mathbf{x}, \mathbf{u}(t)))$ is the pairwise force potential per unit length between two points \mathbf{x} and \mathbf{y} . It is described in terms of its potential function g , given by

$$g(r) = h(r^2) \quad (7)$$

where h is concave. Here ω_2 is the area of the unit disk and $\epsilon^2 \omega_2$ is the area of the horizon $\mathcal{H}_\epsilon(\mathbf{x})$. The influence function $J^\epsilon(|\mathbf{y} - \mathbf{x}|)$ is a measure of the influence that the point \mathbf{y} has on \mathbf{x} . Only points inside the horizon can influence \mathbf{x} so $J^\epsilon(|\mathbf{y} - \mathbf{x}|)$ nonzero for $|\mathbf{y} - \mathbf{x}| < \epsilon$ and zero otherwise. We take J^ϵ to be of the form: $J^\epsilon(|\mathbf{y} - \mathbf{x}|) = J(\frac{|\mathbf{y}-\mathbf{x}|}{\epsilon})$ with $J(r) = 0$ for $r \geq 1$ and $0 \leq J(r) \leq M < \infty$ for $r < 1$.

The displacement field $\mathbf{u}(\mathbf{x}, t)$ evolves according to a nonlocal version of Cauchy’s equations of motion for a continuum body

$$\rho \ddot{\mathbf{u}}^\epsilon(\mathbf{x}, t) = \mathcal{L}^\epsilon(\mathbf{u}^\epsilon)(\mathbf{x}, t) + \mathbf{b}(\mathbf{x}, t), \text{ for } \mathbf{x} \in D. \quad (8)$$

Here $\mathcal{L}^\epsilon(\mathbf{u}^\epsilon)$ is

$$\mathcal{L}^\epsilon(\mathbf{u}^\epsilon) = \int_{\mathcal{H}_\epsilon(\mathbf{x})} \mathbf{f}^\epsilon(\mathbf{y}, \mathbf{x}) d\mathbf{y} \quad (9)$$

and $\mathbf{f}^\epsilon(\mathbf{x}, \mathbf{y})$ is given by

$$\begin{aligned} \mathbf{f}^\epsilon(\mathbf{x}, \mathbf{y}) &= 2\partial_S \mathcal{W}^\epsilon(S(\mathbf{y}, \mathbf{x}, \mathbf{u}^\epsilon(t))) \mathbf{e}_{\mathbf{y}-\mathbf{x}}, \end{aligned} \quad (10)$$

Author Proof

137
138
139
140
141
142
143
144
145
146
147
148
149
150
151
152
153
154
155
156
157

158
159

160
161
162
163
164
165
166

167
168
169

170
171
172
173
174
175
176
177
178
179
180
181
182
183
184
185
186
187
188
189
190
191
192
193
194
195
196

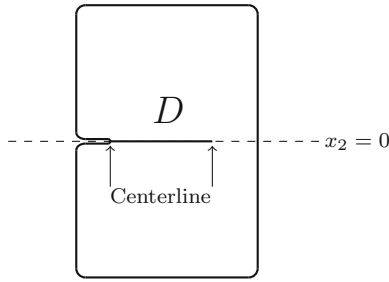


Fig. 3 Failure zone centerline

where

$$\begin{aligned} \partial_S \mathcal{W}^\epsilon(S(\mathbf{y}, \mathbf{x}, \mathbf{u}^\epsilon(t))) \\ = \frac{1}{\epsilon^3 \omega_2} \frac{J^\epsilon(|\mathbf{y} - \mathbf{x}|)}{|\mathbf{y} - \mathbf{x}|} \partial_S g(\sqrt{|\mathbf{y} - \mathbf{x}|} S(\mathbf{y}, \mathbf{x}, \mathbf{u}^\epsilon(t))). \end{aligned} \quad (11)$$

The dynamics is complemented with the initial data

$$\mathbf{u}^\epsilon(\mathbf{x}, 0) = \mathbf{u}_0(\mathbf{x}), \quad \partial_t \mathbf{u}^\epsilon(\mathbf{x}, 0) = \mathbf{v}_0(\mathbf{x}), \quad (12)$$

and the appropriate traction and Dirichlet boundary conditions described in Sect. 5.

2.1 Failure Zone - Process Zone

The failure zone represents the crack in the nonlocal model. It is characterized by the failure zone centerline. The failure zone centerline starts at the notch and propagates into the interior of the specimen. The force between two points \mathbf{x} and \mathbf{y} separated by the failure zone centerline is zero. The centerline is shown in Fig. 3 and the failure zone is the grey region in Fig. 4. For the boundary conditions chosen here failure is in tension and confined to a neighborhood of the $x_2 = 0$ axis of width 2ϵ . Just in front of the failure zone is the process zone where the force between two points \mathbf{x} and \mathbf{y} on either side of the $x_2 = 0$ axis is decreasing with increasing strain. At the leading edge of the crack one sees force softening between points \mathbf{x} and \mathbf{y} and as the crack centerline moves forward passing between \mathbf{x} and \mathbf{y} the force between \mathbf{x} and \mathbf{y} decreases to zero, see Fig. 4. It needs to be stressed the failure zone and process zone emerge from the nonlocal dynamics and are not prescribed. For example see Sect. 5, Fig. 10.

3 Fracture toughness and elastic properties for the cohesive model: as specified through the force potential

For finite horizon $\epsilon > 0$ the fracture toughness and elastic moduli are recovered directly from the cohesive strain potential $\mathcal{W}^\epsilon(S(\mathbf{y}, \mathbf{x}, \mathbf{u}(t)))$. Here the fracture toughness \mathcal{G}_c is defined to be the energy per unit length required eliminate force between each point \mathbf{x} and \mathbf{y} on either side of a line in \mathbb{R}^2 . In this case the line is the $x_2 = 0$ axis. Because of the finite length scale of interaction only the force between pairs of points within an ϵ distance from the line are considered. The fracture toughness \mathcal{G}_c is calculated in Lipton (2016). Proceeding as in Silling and Askari (2005) we have

$$\mathcal{G}_c = 2 \int_0^\epsilon \int_z^\epsilon \int_0^{\arccos(z/\zeta)} \mathcal{W}^\epsilon(S_+) \zeta^2 d\psi d\zeta dz \quad (13)$$

where $\zeta = |\mathbf{y} - \mathbf{x}|$, see Fig. 5. Substitution of $\mathcal{W}^\epsilon(S(\mathbf{y}, \mathbf{x}, \mathbf{u}(t)))$ given by (6) into (13) delivers

$$\mathcal{G}_c = \frac{4}{\pi} \int_0^1 h(S_+^2) r^2 J(r) dr. \quad (14)$$

It is evident from this calculation that the fracture toughness is the same for all choice of horizons. This provides the rational behind the ϵ scaling of the potential (6) for the cohesive model. Moreover the layer width on either side of the crack centerline over which the force is applied to create new surface tends to zero with ϵ . In this way ϵ can be interpreted as a parameter associated with the size of the failure zone of the material. Equation (14) gives a way to calibrate the function h that specifies the potential (7) when \mathcal{G}_c is given.

Further calibration of h is possible using the elastic moduli of the material. To calibrate h we relate elastic moduli of the material to the cohesive potential $\mathcal{W}^\epsilon(S(\mathbf{y}, \mathbf{x}, \mathbf{u}(t)))$. When the horizon is sufficiently small we suppose the displacement inside $\mathcal{H}_\epsilon(\mathbf{x})$ is affine, that is, $\mathbf{u}(\mathbf{x}) = F\mathbf{x}$ where F is a constant matrix. For small strains, i.e., $S = F e \cdot e \ll S_c$, a Taylor series expansion at zero strain shows that the strain potential is linear elastic to leading order and characterized by elastic moduli μ and λ associated with a linear elastic isotropic material

$$\begin{aligned} W(\mathbf{x}) &= \int_{\mathcal{H}_\epsilon(\mathbf{x})} |\mathbf{y} - \mathbf{x}| \mathcal{W}^\epsilon(S(\mathbf{y}, \mathbf{x}, \mathbf{u})) d\mathbf{y} \\ &= \mu |F|^2 + \frac{\lambda}{2} |Tr\{F\}|^2 + O(\epsilon |F|^4). \end{aligned} \quad (15)$$

Author Proof

Fig. 4 The failure zone is the grey shaded region and the process zone is the clear region inside the contour

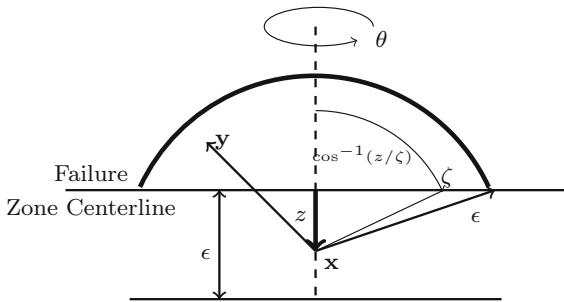
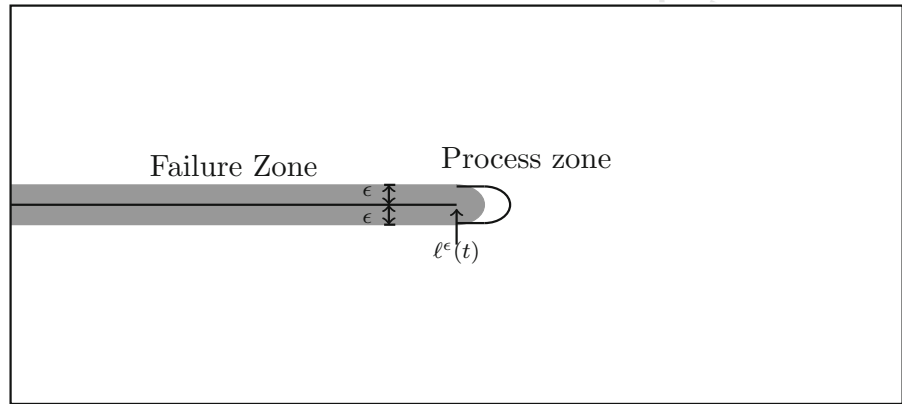


Fig. 5 Evaluation of fracture toughness G_c . For each point x along the dashed line, $0 \leq z \leq \epsilon$, the work required to break the interaction between x and y in the spherical cap is summed up in (13) using spherical coordinates centered at x . This summation is done on both sides of the failure zone centerline

268 The elastic moduli λ and μ are calculated directly from
269 the strain energy density and are given by

$$270 \quad \mu = \lambda = M \frac{1}{4} h'(0), \quad (16)$$

271 where the constant $M = \int_0^1 r^2 J(r) dr$. The elasticity
272 tensor is given by

$$273 \quad \mathbb{C}_{ijkl} = 2\mu \left(\frac{\delta_{ik}\delta_{jl} + \delta_{il}\delta_{jk}}{2} \right) + \lambda \delta_{ij}\delta_{kl}. \quad (17)$$

274 When μ is specified $h'(0)$ is determined by (16). For
275 the simple potentials considered here the elasticity cor-
276 responds to materials with Poisson's ratio 1/4, i.e.,
277 $\lambda = \mu$. It is noted that we are free to consider other
278 multi well potentials and general choices of Poisson's
279 ratios [Jha and Lipton \(2019b\)](#); these correspond to state
280 based peridynamic models [Silling et al. \(2007\)](#).

4 Kinetic relation from nonlocal dynamics

281

In this section we show that the well known kinetic
282 relation for the velocity of the crack tip, [Freund \(1990\)](#),
283 follows from the nonlocal model in the limit of vanishing
284 horizon in two different ways. We begin by defining
285 the kinetic energy density by $T^\epsilon = \rho |\dot{\mathbf{u}}^\epsilon(\mathbf{x}, t)|^2 / 2$ and
286 the stress work density for the nonlocal model given by
287 $W^\epsilon(\mathbf{x}) = \int_{\mathcal{H}_\epsilon(\mathbf{x})} |\mathbf{y} - \mathbf{x}| \mathcal{W}^\epsilon(S(\mathbf{y}, \mathbf{x}, \mathbf{u}^\epsilon(t))) d\mathbf{y}$.
288

4.1 Rate of internal energy change inside a domain containing the crack tip

289

290

Note that for the nonlocal model the same equation
291 applies everywhere in the body. Because of this we
292 can calculate the time rate of change of internal energy
293 of a domain containing the crack tip and pass to the
294 limit of local interactions. Fix a contour Γ_δ of diameter
295 δ surrounding the domain $\mathcal{P}_\delta(t)$ containing the tip of
296 the failure zone for the local model, see [Fig. 6](#). Recall
297 that the line centered within the failure zone running
298 from the notch to the leading edge of the failure zone
299 is called the failure zone center line, see [Fig. 3](#). We
300 investigate power balance in regions containing the tip
301 of the failure zone. We suppose $\mathcal{P}_\delta(t)$ is moving with
302 the crack tip velocity $V^\epsilon(t)$ along the horizontal axis.
303 A direct calculation given in [Sect. 6](#) establishes the
304 following explicit formula for the rate of change in
305 internal energy inside the domain containing the edge
306 of the failure zone.
307

Rate of change of internal energy for a region con-
308 taining the crack tip for the nonlocal model:
309

$$310 \quad \frac{d}{dt} \int_{\mathcal{P}_\delta(t)} T^\epsilon + W^\epsilon d\mathbf{x} = I^\epsilon(\Gamma_\delta(t)) \quad (18)$$

310

Author Proof

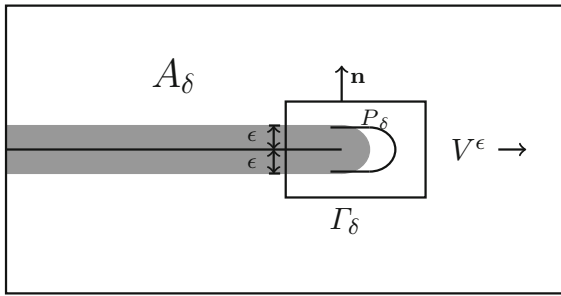


Fig. 6 Contour Γ_δ surrounding the domain P_δ moving with the velocity V^ϵ of the failure zone in grey and process zone

with

$$I^\epsilon(\Gamma_\delta(t)) = \int_{\Gamma_\delta(t)} (T^\epsilon + W^\epsilon)V^\epsilon \mathbf{e}^1 \cdot \mathbf{n} \, ds - E^\epsilon(\Gamma_\delta(t)), \tag{19}$$

where \mathbf{n} is the outward directed unit normal, ds is an element of arc length, and \mathbf{e}^1 is the unit vector pointing in the direction of crack propagation. The rate of elastic energy flowing into the domain surrounding the crack tip is

$$E^\epsilon(\Gamma_\delta(t)) = \int_{A_\delta(t)} \int_{\mathcal{H}_\epsilon(\mathbf{x}) \cap \mathcal{P}_\delta(t)} \partial_S \mathcal{W}^\epsilon(S(\mathbf{y}, \mathbf{x}, \mathbf{u}^\epsilon)) \mathbf{e}_{\mathbf{y}-\mathbf{x}} \cdot (\dot{\mathbf{u}}^\epsilon(\mathbf{x}) + \dot{\mathbf{u}}^\epsilon(\mathbf{y})) \, d\mathbf{y}d\mathbf{x}, \tag{20}$$

where $A_\delta(t)$ is the part of D exterior to $\mathcal{P}_\delta(t)$. These relations follow directly from the nonlocal Cauchy's equations of motion (8), this is shown in Sect. 6. Equation (18) gives the following energy criterion for local power balance:

Local power balance of a neighborhood containing the crack tip is given by the stationarity of its internal energy with respect to time.

The stress work density flowing into the moving domain is related to fracture toughness by

$$\int_{\Gamma_\delta(t)} W^\epsilon V^\epsilon \mathbf{e}^1 \cdot \mathbf{n} \, ds = -\mathcal{G}_c V^\epsilon(t) + O(\delta). \tag{21}$$

and

$$\int_{\Gamma_\delta(t)} T^\epsilon V^\epsilon \mathbf{e}^1 \cdot \mathbf{n} \, ds = O(\delta). \tag{22}$$

These identities are obtained in Sect. 7. One recalls that the stress power is that part of the externally supplied power which is not converted into kinetic energy. This is corroborated by the numerical experiments provided in Sect. 5.

When the horizon goes to zero we get for $V^\epsilon \mathbf{e}^1 \rightarrow V \mathbf{e}^1$,

$$\lim_{\epsilon \rightarrow 0} \int_{\Gamma_\delta(t)} W^\epsilon V^\epsilon \mathbf{e}^1 \cdot \mathbf{n} \, ds = -\mathcal{G}_c V(t), \tag{23}$$

$$\lim_{\epsilon \rightarrow 0} E^\epsilon(\Gamma_\delta(t)) = - \int_{\Gamma_\delta} \mathbb{C} \mathcal{E} \mathbf{u}^0 \mathbf{n} \cdot \dot{\mathbf{u}}^0 \, ds + O(\delta),$$

where $\mathbb{C} \mathcal{E} \mathbf{u}^0 \mathbf{n} \cdot \dot{\mathbf{u}}^0$ is the energy flux into P_δ . The change in internal energy inside the domain containing the crack tip is given by:

$$\lim_{\epsilon \rightarrow 0} \frac{d}{dt} \int_{\mathcal{P}_\delta(t)} T^\epsilon + W^\epsilon \, d\mathbf{x} = \int_{\Gamma_\delta} \mathbb{C} \mathcal{E} \mathbf{u}^0 \mathbf{n} \cdot \dot{\mathbf{u}}^0 \, ds - \mathcal{G}_c V(t) + O(\delta). \tag{24}$$

Off the crack the displacement \mathbf{u}^0 satisfies Cauchy's equations of motion for a continuum body

$$\rho \ddot{\mathbf{u}}^0 = \text{div}(\mathbb{C} \mathcal{E} \mathbf{u}^0) + \mathbf{b} \tag{25}$$

where $\mathcal{E}_{ij} = 1/2(\mathbf{u}_{i,j}^0 + \mathbf{u}_{j,i}^0)$ is the symmetrized gradient Lipton (2014, 2016). The crack flanks are traction free and \mathbf{u}^0 satisfies boundary and initial conditions see Lipton and Jha (2020).

For $\mathcal{F} = \lim_{\delta \rightarrow 0} \int_{\Gamma_\delta} \mathbb{C} \mathcal{E} \mathbf{u}^0 \mathbf{n} \cdot \dot{\mathbf{u}}^0 \, ds$ we get

$$\lim_{\delta \rightarrow 0} \lim_{\epsilon \rightarrow 0} \frac{d}{dt} \int_{\mathcal{P}_\delta(t)} T^\epsilon + W^\epsilon \, d\mathbf{x} + \mathcal{G}_c V = \mathcal{F}. \tag{26}$$

Power balance gives

$$\lim_{\delta \rightarrow 0} \lim_{\epsilon \rightarrow 0} \frac{d}{dt} \int_{\mathcal{P}_\delta(t)} T^\epsilon + W^\epsilon \, d\mathbf{x} = 0, \tag{27}$$

and from Atkinson and Eshelby (1965), Kostrov and Nikitin (1970), Freund (1972), and Willis (1975) the semi explicit kinetic relation connecting the energy flux into the crack tip to the crack velocity follows from (26) and is of the form given by Freund and Clifton (1974)

$$\mathcal{G}_c = \frac{\mathcal{F}}{V} = \frac{1+\nu}{E} \frac{V^2}{c_s^2 D} \alpha_t K_I^2(t), \tag{28}$$

where ν is the Poisson's ratio, E is the Young modulus V is the crack velocity, c_s is the shear wave speed, $c_l = (\lambda + 2\mu/\rho)^{1/2}$ is the longitudinal wave speed, $D = 4\alpha_s \alpha_l - (1 + \alpha_s^2)^2$, and $\alpha_s = (1 - V^2/c_s^2)^{1/2}$, $\alpha_l = (1 - V^2/c_l^2)^{1/2}$. Here $K_I(t)$ is the mode I dynamic stress intensity factor and depends on the details of the loading and is not explicit.

In summary (24) and (26) are recovered directly from (8) and are a consequence of the nonlocal dynamics in the $\epsilon = 0$ limit. The recovery is possible since the nonlocal model is well defined over the failure zone. The rate of change in energy (18) and its limit (24) are calculated in Sects. 6 and 7.

Author Proof

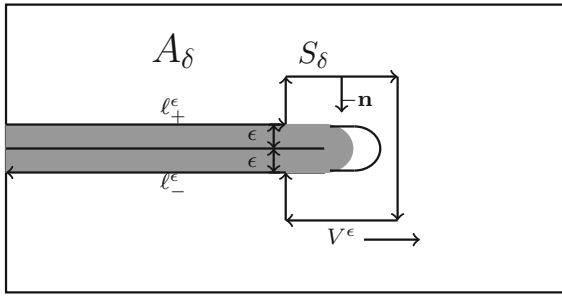


Fig. 7 The contour S_δ surrounding the tip of the failure zone (in gray) and process zone moving with velocity V^ϵ

4.2 Local power balance for translation invariant displacement in the neighborhood of the crack tip.

In this section we consider a constant velocity crack for our peridynamic model and suppose that the displacement is translation invariant in the neighborhood of the crack tip. These assumptions are standard in LEFM Rice (1968b), Sih (1968), Irwin (1967), Freund and Clifton (1974), Nillison (1974). For this case we show that the change in the internal energy of the neighborhood surrounding the crack tip is zero. So energy balance holds for the peridynamic model. To see this consider the translation invariant displacement field of the form $\mathbf{u}^\epsilon(\mathbf{x}, t) = \mathbf{u}^\epsilon(\mathbf{x} - tV\mathbf{e}^1)$ where t is time and V is the constant crack speed directed along the positive x_1 axis. It follows that the stress power and rate of change in kinetic energy inside \mathcal{P}_δ are given by

$$\begin{aligned} \dot{W}^\epsilon &= -\partial_{x_1} W^\epsilon V \\ \dot{T}^\epsilon &= -\partial_{x_1} T^\epsilon V. \end{aligned} \tag{29}$$

So from the divergence theorem we get

$$\begin{aligned} \int_{\mathcal{P}_\delta(t)} \dot{T}^\epsilon + \dot{W}^\epsilon \, d\mathbf{x} \\ = - \int_{\Gamma_\delta(t)} (T^\epsilon + W^\epsilon) V^\epsilon \mathbf{e}^1 \cdot \mathbf{n} \, ds, \end{aligned} \tag{30}$$

and by Reynolds transport theorem (54) we discover the nonlocal model gives local power balance, i.e.,

$$\frac{d}{dt} \int_{\mathcal{P}_\delta(t)} T^\epsilon + W^\epsilon \, d\mathbf{x} = 0. \tag{31}$$

From this together with (18), (30) we conclude that

$$\int_{\Gamma_\delta(t)} (T^\epsilon + W^\epsilon) V^\epsilon \mathbf{e}^1 \cdot \mathbf{n} \, ds - E^\epsilon(\Gamma_\delta(t)) = 0, \tag{32}$$

and from (21) our peridynamic model gives

$$\mathcal{G}_c V = -E^\epsilon(\Gamma_\delta(t)) + O(\delta). \tag{33}$$

On passing to the zero horizon limit in the nonlocal dynamics we see that local power balance for constant velocity cracks modeled by LEFM is given by

Local power balance for LEFM:

$$\mathcal{G}_c V = \lim_{\delta \rightarrow 0} \int_{\Gamma_\delta} \mathbb{C} \mathcal{E} \mathbf{u}^0 \mathbf{n} \cdot \dot{\mathbf{u}}^0 \, ds. \tag{34}$$

The local power balance for LEFM has been predicted here using the nonlocal model.

4.3 The peridynamic J integral and Linear Elastic Fracture Mechanics

For LEFM the elastic field near the crack tip is derived from the local Cauchy's equations of motion for a continuum body. This gives the flow of elastic energy into the crack tip, Freund (1990). On the other hand the kinetic relation for LEFM does not follow from the local Cauchy's equation of motion alone. Instead the kinetic relation for LEFM follows from Mott's hypothesis Mott (1948) on the balance of elastic energy flowing into the crack tip and power needed to create new fracture surface Freund (1990). In this section we will proceed like is done in the local theory but obtain the J integral for the nonlocal model and compare with the previous results. We compute the time rate of change of the internal energy of the domain $A_\delta(t)$ surrounding the crack tip inside the contour shown in Fig. 7. Calculation as in Sect. 7 shows that the energy flux from A_δ into the flanks of the failure zone ℓ_\pm^ϵ is zero so the energy flux through the surface S_δ of diameter δ is the energy flow into the tip of the damage zone given by $J^\epsilon(S_\delta(t))$ where

$$\begin{aligned} J^\epsilon(S_\delta(t)) &= - \int_{S_\delta(t)} (T^\epsilon + W^\epsilon) V^\epsilon \mathbf{e}^1 \cdot \mathbf{n} \, ds \\ &\quad + E^\epsilon(S_\delta(t)), \end{aligned} \tag{35}$$

here \mathbf{n} is the outward directed unit normal. The rate of elastic energy flowing into in the domain surrounding the crack tip is

$$\begin{aligned} E^\epsilon(S_\delta(t)) &= \int_{A_\delta(t)} \int_{\mathcal{H}_\epsilon(\mathbf{x}) \cap \mathcal{Q}_\delta(t)} \partial_S \mathcal{W}^\epsilon(S(\mathbf{y}, \mathbf{x}, \mathbf{u}^\epsilon)) \mathbf{e}_{\mathbf{y}-\mathbf{x}} \\ &\quad \cdot (\dot{\mathbf{u}}^\epsilon(\mathbf{x}) + \dot{\mathbf{u}}^\epsilon(\mathbf{y})) \, d\mathbf{y} d\mathbf{x}. \end{aligned} \tag{36}$$

Author Proof

435 When the horizon goes to zero a calculation as in Sect. 7
436 shows,

$$\lim_{\epsilon \rightarrow 0} \int_{S_\delta(t)} (T^\epsilon + W^\epsilon) V^\epsilon \mathbf{e}^1 \cdot \mathbf{n} \, ds = O(\delta),$$

$$\lim_{\epsilon \rightarrow 0} E^\epsilon(S_\delta(t)) = - \int_{S_\delta} \mathbb{C} \mathcal{E} \mathbf{u}^0 \mathbf{n} \cdot \dot{\mathbf{u}}^0 \, ds, \quad (37)$$

438 and the local limit of the peridynamic J integral is given
439 by

$$440 \quad J(S_\delta(t)) = - \int_{S_\delta} \mathbb{C} \mathcal{E} \mathbf{u}^0 \mathbf{n} \cdot \dot{\mathbf{u}}^0 \, ds + O(\delta) \quad (38)$$

441 and on taking $\delta = 0$ we recover the total energy flux into
442 the crack tip as in LEFM. Note that (38) differs from
443 (24) since S_δ does not cross the failure zone. Formula
444 (38) is the well known J integral of LEFM introduced
445 in Rice (1968a), and developed for dynamics Atkinson
446 and Eshelby (1965), Freund (1972), and Sih (1970).
447 Applying energy balance and using the general form
448 of the elastic fields near the crack tip for samples of
449 infinite extent Atkinson and Eshelby (1965), Kostrov
450 and Nikitin (1970), Freund (1972), and Willis (1975)
451 we recover the crack tip kinetic relation (28).

452 Alternate versions of the peridynamic J integral have
453 been deduced for dynamic fracture problems in Silling
454 and Lehoucq (2010) using balance laws. For quasi-
455 static fracture problems the work of Hu et al. (2012),
456 derive a J integral using an infinitesimal virtual crack
457 extension and Stenström and Eriksson (2019) acceler-
458 ate the numerical calculation of the J integral using the
459 peridynamic displacement field. The dynamic J integral
460 developed here is derived from the equation of
461 motion using integration by parts and naturally agrees
462 with Silling and Lehoucq (2010). However the explicit
463 form is different and follows from a suitable change
464 of variables. In addition the “crack” for the nonlocal
465 model is not artificially assumed infinitesimally thin as
466 in other approaches but instead we use the fact that it
467 has a thickness that is twice the peridynamic horizon.

468 To summarize the approach of Sect. 4.1 is self
469 contained and follows exclusively from the nonlocal
470 Cauchy equation of motion. While the approach of
471 Sect. 4.3 reflects the classic approach and uses the non-
472 local model to compute the elastic energy only. It is then
473 equated to the energy required to create new fracture
474 surface invoking Mott’s hypothesis as is done with the
475 local theory.

5 Numerical simulation and analysis 476

477 The principal point of peridynamic modeling is that
478 crack motion is part of the solution and emerge from
479 the nonlocal dynamics. This is the hallmark of peridy-
480 namic modeling Silling (2000), Ha and Bobaru (2010).
481 In this section, we provide a numerical simulation using
482 the cohesive dynamics given by (8) to see that a crack
483 moving at constant speed satisfies energy balance. The
484 numerical computation also shows that the stress work
485 flux is nearly equal to the energy release rate as antici-
486 pated by the theory, see (21), (22), (23).

5.1 Setup 487

488 We consider a sample of material with Young’s modu-
489 lus $E = 88$ kPa, Poisson’s ratio $\nu = 0.25$, and material
490 density $\rho = 1011.2$ kg/m³. The Rayleigh wave speed
491 and shear wave speed for the sample are $c_R = 5.502$
492 m/s and $c_s = 5.9$ m/s respectively. The numerical simu-
493 lation is motivated by the experiments carried out in
494 Goldman et al. (2010) and the material domain, hori-
495 zon, discretization, and boundary conditions are shown
496 in Fig. 8. In this work we assume plane stress condi-
497 tions. We consider a pre-cracked specimen as shown
498 in Fig. 8. The pre-crack is of length $l = 3$ mm. The
499 critical energy release rate is taken to be $\mathcal{G}_c = 20$ J/m².

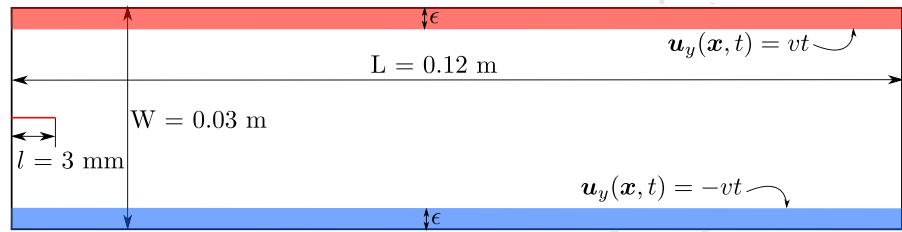
500 The force potential is $g(r) = c(1 - \exp[-\beta r^2])$,
501 where c, β are constants. The influence function is of
502 the form $J(r) = 1 - r$. Equations (14), (16) are used
503 to calibrate the values of the parameters c, β . For the
504 material properties listed above we get $c = 15.705$,
505 $\beta = 8965.378$. We define the damage $Z(\mathbf{x})$ at a mate-
506 rial point \mathbf{x} as follows:

$$507 \quad Z(\mathbf{x}) = \sup_{\mathbf{y} \in \mathcal{H}_\epsilon(\mathbf{x})} \frac{|S(\mathbf{y}, \mathbf{x}, \mathbf{u}(t))|}{S_c(\mathbf{y}, \mathbf{x})}. \quad (39)$$

508
509 A value $Z > 1$ implies that there are neighboring points
510 \mathbf{y} for which the bond-strain between points \mathbf{y} and \mathbf{x} lies
511 above the critical strain.

512 We consider a uniform discretization and offset the
513 crack vertically by $h/100$ where $h = 0.125$ mm is
514 the mesh size so that the crack line is not on the grid
515 line. For temporal discretization, we consider velocity-
516 verlet scheme with time step size $\Delta t = 2.2$ μ s and final
517 time $T = 1.1$ s. For mesh convergence, we rely on our
518 earlier work Jha and Lipton (2019b) where a similar

Fig. 8 Setup for steady state crack propagation experiment. Here $\epsilon = 0.75$ mm and $v = 1.475$ mm/s. Domain is uniformly discretized with mesh size $h = \epsilon/6 = 0.125$ mm



519 setup was considered and convergence with respect to
 520 the mesh was shown. To see if the simulation changes
 521 when using an unstructured mesh, we ran the same
 522 problem on unstructured mesh consisting of linear tri-
 523 angle elements. We first obtained the mesh using Gmsh
 524 library and then computed the nodal volume associated
 525 to each vertex in the mesh. Pairs of vertices and vol-
 526 umes form the particle mesh. The results were similar
 527 to the case of uniform discretization.

528 We choose crack tip location as a measure of conver-
 529 gence of the temporal discretization. Here the crack tip
 530 is recovered as a post processing step. In order to find
 531 the crack tip at any given time step we search the sim-
 532 ulation output data for vertices with damage Z greater
 533 than 1 and the crack tip is the vertex such that

- 534 – No other vertex on the right side of the selected
- 535 vertex exists with $Z > 1$.

536 To illustrate time convergence, we consider the same
 537 simulation but using a smaller time step $\Delta t = 1.1 \mu\text{s}$.
 538 The crack tip position is compared for the two different
 539 time steps at times $t = 0.9603, 0.9647, 0.9801$ s. Here
 540 the x-coordinates of the crack tip for $\Delta t = 2.2 \mu\text{s}$ and
 541 $\Delta t = 1.1 \mu\text{s}$ are given by 0.011057, 0.02456, 0.072951
 542 m and 0.011018, 0.024525, 0.072939 m respectively.
 543 The simulation for the time step $\Delta t = 2.2$ is shown in
 544 Fig. 9 at times $t = 0.9603, 0.9647, 0.9801$ s.

545 Crack velocities are computed over a longer time
 546 step $\overline{\Delta t}$, i.e. *Crack velocity* = *Distance traveled*
 547 *over timestep* / $\overline{\Delta t}$. Here $\overline{\Delta t} = 0.0022$ s while the time
 548 step used in the simulation is $\Delta t = 2.2 \mu\text{s}$. The choice
 549 of $\overline{\Delta t}$ smooths out the high frequency velocity fluctu-
 550 ations due to bond breaking and delivers an averaged
 551 crack velocity over an interval of length $\overline{\Delta t}$.

552 When labeling plots we will apply the following
 553 notation:

$$554 \quad WV := \int_{\Gamma_\delta} W^\epsilon V^\epsilon \cdot nds,$$

$$555 \quad F_{pd} := -E^\epsilon(\Gamma_\delta)$$

$$\dot{E} := \frac{d}{dt} \int_{\mathcal{P}_\delta} T^\epsilon + W^\epsilon dx, \quad (40)$$

556 where V^ϵ is the crack velocity. All plotted quantities
 557 are in units of Joules/s. We will also display the total
 558 fracture energy at time t , denoted by PE , see (41), and
 559 the total energy released by a crack of length l , given
 560 by $GE = l \times \mathcal{G}_c$.
 561
 562

5.2 Results

563
 564 The plot of crack velocity and deformation field sur-
 565 rounding the crack tip centerline at three selected times
 566 are shown in Fig. 9. Damage in the reference configura-
 567 tion is plotted in Fig. 10. The figure shows that damage
 568 is localized and corresponds to the crack in the nonlo-
 569 cal model and is of width $2(\epsilon + h)$. The crack veloc-
 570 ity history given by Fig. 9 is in qualitative agreement
 571 with experimental results (Goldman et al. 2010, Figure
 572 2). There is an initial increase in crack speed, but as
 573 waves reflect back from the boundary onto the crack
 574 tip the velocity becomes roughly constant. To display
 575 the crack opening displacement and the deformation of
 576 the specimen we have added the displacement field at
 577 the node to its nodal location. This is done for all nodal
 578 points in the specimen, see Fig. 9.

579 Next, we focus on regime of near constant crack
 580 speed corresponding to the time interval $[0.9647, 0.9801]$.
 581 As predicted from theory, see (21), $-WV$ agrees with
 582 $V\mathcal{G}_c$ see Fig. 11. The simulation also shows that the
 583 time rate of change in kinetic energy near the crack tip
 584 is small and F_{pd} is close to $V\mathcal{G}_c$ see Fig. 11. The bot-
 585 tom Fig. in 11 shows that the rate of total energy \dot{E} in
 586 the constant crack speed regime is close to zero.

587 We compute the peridynamic energy of the failure
 588 zone and compare it with the classic fracture energy.
 589 For a crack of length at time t given by $l(t)$, the classic
 590 fracture energy (GE) is $GE(t) = G_c \times l(t)$. Recall the
 591 failure zone at time t is denoted by

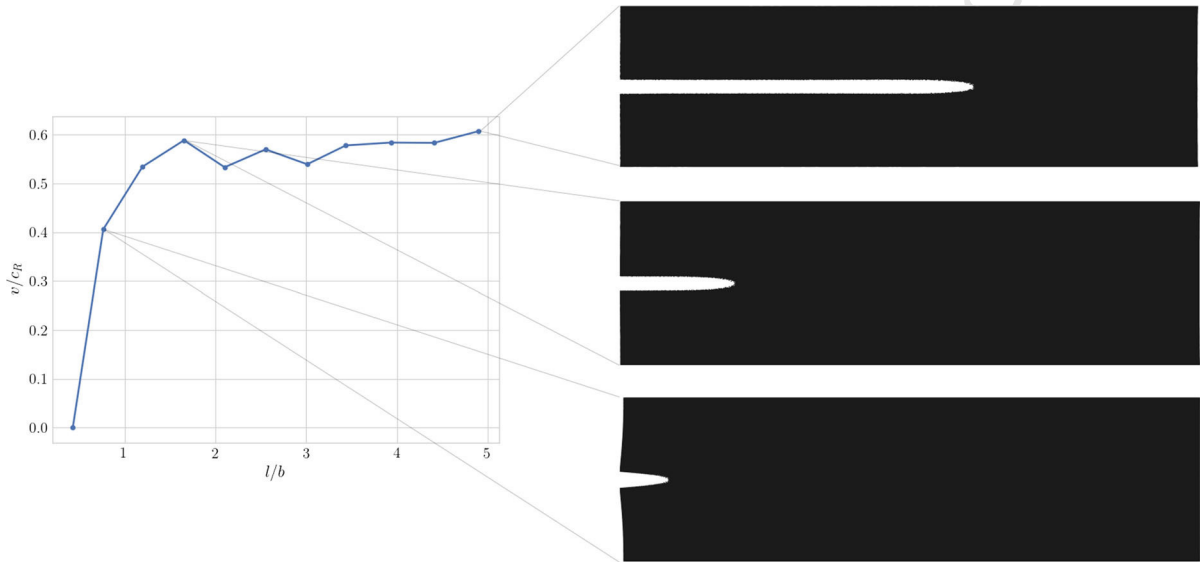


Fig. 9 Left: Crack velocity vs crack length. $b = 0.015$ m is the half width of the domain. $c_R = 5.502$ m/s is the Rayleigh wave speed. The crack velocity approaches steady state value of 0.6 which is consistent with the experimental result in Goldman et al. (2010); Bouchbinder et al. (2014). This is due to the

fact that crack feels the boundary and wave reflection from the boundary obstructs crack to acquire more velocity. Right: Crack opening displacement and deformation in the specimen at times $t = 0.9603, 0.9647, 0.9801$ s

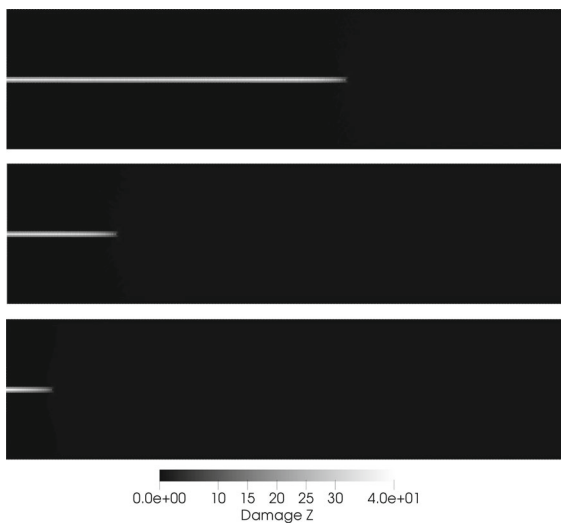


Fig. 10 The crack together with process zone is given for $Z > 1$ in the reference configuration at times $t = 0.9603, 0.9647, 0.9801$ s. Here the points where $Z > 1$ are shaded white all other points are shaded black. The crack is a thin region of thickness $2(\epsilon + h)$

$$PE(t) = \int_{FZ^\epsilon(t)} \left[\frac{1}{\epsilon^d \omega_d} \int_{H_\epsilon(x)} |y - x| \mathcal{W}^\epsilon(S(y, x, u)) dy \right] dx. \tag{41}$$

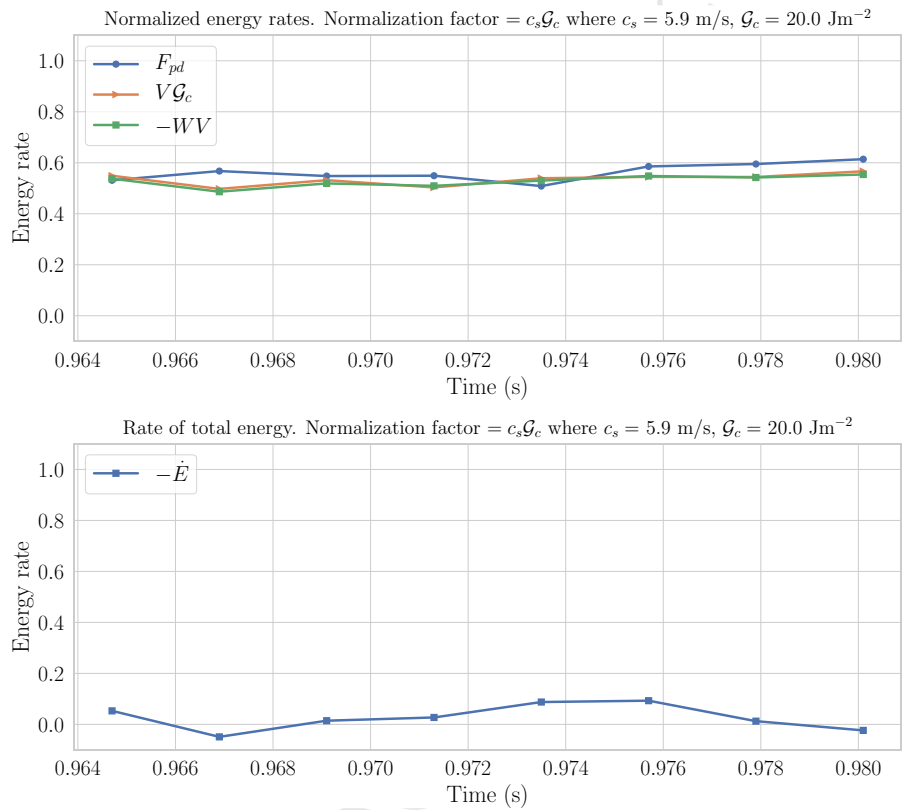
The peridynamic fracture energy is compared to the classic fracture energy in Fig. 12 and is seen to be nearly identical.

6 Change in internal energy on subdomains containing the crack tip for the nonlocal model

In this section we recover the rate of change of internal energy (18) using the nonlocal version of Cauchy's equations of motion for a continuum body given by (8). Consider the rectangular contour $\Gamma_\delta(t)$ of diameter δ bordering the domain $\mathcal{P}_\delta(t)$ containing the crack tip. We suppose $\mathcal{P}_\delta(t)$ is moving with the crack tip speed $V^\epsilon(t)$ see Fig. 6. It will be shown that the rate of change of energy inside $\mathcal{P}_\delta(t)$ for the nonlocal dynamics is given by (18). We start by introducing a nonlocal divergence theorem applied to the case at hand. To expedite taking $\epsilon \rightarrow 0$ limits in the next section we make the change of variables $y = x + \epsilon\xi$ where ξ

$FZ^\epsilon(t)$ and the peridynamic fracture energy (PE) is given by

Fig. 11 Top: Normalized rate of energies given by F_{pd} , $-WV$ and LFM rate $V \times \mathcal{G}_c$. Bottom: Negative of rate of total contour energy, $-\dot{E}$. Here energy rates are divided by $c_s \mathcal{G}_c$, where $c_s = 5.9 \text{ m/s}$ is the shear wave speed and $\mathcal{G}_c = 20.0 \text{ J/m}^2$ is the critical energy release rate. Plots are at time steps in the constant crack speed time interval $[0.9647, 0.9801]$. In both plots, the limits in y-axis are taken as $[-0.1, 1.0]$ where the upper limit is the normalized energy rate associated to crack moving at shear wave speed



614 belongs to the unit disk at the origin $\mathcal{H}_1(0) = \{|\xi| < 1\}$
 615 and $\mathbf{e} = \xi/|\xi|$. The strain is written

$$\frac{\mathbf{u}^\epsilon(\mathbf{x} + \epsilon\xi) - \mathbf{u}^\epsilon(\mathbf{x})}{\epsilon|\xi|} := D_e^{\epsilon|\xi|} \mathbf{u}^\epsilon, \text{ and} \tag{42}$$

$$S(\mathbf{y}, \mathbf{x}, \mathbf{u}^\epsilon(t)) = D_e^{\epsilon|\xi|} \mathbf{u}^\epsilon \cdot \mathbf{e},$$

617 and the work done in straining the material between
 618 points \mathbf{y} and \mathbf{x} given by $|\mathbf{y} - \mathbf{x}| \partial_S \mathcal{W}^\epsilon(S(\mathbf{y}, \mathbf{x}, \mathbf{u}^\epsilon(t)))$
 619 transforms in the new variables to

$$\begin{aligned} & \epsilon|\xi| \partial_S \mathcal{W}^\epsilon(D_e^{\epsilon|\xi|} \mathbf{u}^\epsilon \cdot \mathbf{e}) \\ &= \frac{2|\xi|J(|\xi|)}{\epsilon^2 \omega_2} h'(\epsilon|\xi| |D_e^{\epsilon|\xi|} \mathbf{u}^\epsilon \cdot \mathbf{e}|^2) D_e^{\epsilon|\xi|} \mathbf{u}^\epsilon \cdot \mathbf{e}. \end{aligned} \tag{43}$$

622 We will use the following nonlocal divergence theorem.
 623 Nonlocal divergence theorem:

$$\begin{aligned} & \epsilon^2 \int_{P_\delta(t)} \int_{\mathcal{H}_1(0)} D_e^{\epsilon|\xi|} \left[\epsilon|\xi| \partial_S \mathcal{W}^\epsilon(D_e^{\epsilon|\xi|} \mathbf{u}^\epsilon \cdot \mathbf{e}) \mathbf{w}(\mathbf{x}) \cdot \mathbf{e} \right] d\xi d\mathbf{x} \\ &= \epsilon^2 \int_{H_1(0)} \int_{(P_\delta(t) - \epsilon\xi) \setminus P_\delta(t)} \partial_S \mathcal{W}^\epsilon(D_e^{\epsilon|\xi|} \mathbf{u}^\epsilon \cdot \mathbf{e}) \mathbf{w}(\mathbf{x}) \cdot \mathbf{e} d\mathbf{x} d\xi \\ & \quad - \epsilon^2 \int_{H_1(0)} \int_{P_\delta(t) \setminus (P_\delta(t) - \epsilon\xi)} \partial_S \mathcal{W}^\epsilon(D_e^{\epsilon|\xi|} \mathbf{u}^\epsilon \cdot \mathbf{e}) \mathbf{w}(\mathbf{x}) \cdot \mathbf{e} d\mathbf{x} d\xi. \end{aligned} \tag{44}$$

This identity follows on applying the definition of $D_e^{\epsilon|\xi|} \varphi = (\varphi(\mathbf{x} - \epsilon\xi) - \varphi(\mathbf{x}))/\epsilon|\xi|$ for scalar fields φ and Fubini's theorem. When convenient we set $A_\delta(t) = D \setminus P_\delta(t)$ and rewrite the last two terms of (44) in \mathbf{x} and \mathbf{y} variables to get

$$\begin{aligned} & \epsilon^2 \int_{P_\delta(t)} \int_{\mathcal{H}_1(0)} D_e^{\epsilon|\xi|} \left[\epsilon|\xi| \partial_S \mathcal{W}^\epsilon(D_e^{\epsilon|\xi|} \mathbf{u}^\epsilon \cdot \mathbf{e}) \mathbf{w} \cdot \mathbf{e} \right] d\xi d\mathbf{x} \\ &= \int_{A_\delta(t)} \int_{\mathcal{H}_\epsilon(\mathbf{x}) \cap P_\delta(t)} \partial_S \mathcal{W}^\epsilon(S(\mathbf{y}, \mathbf{x}, \mathbf{u}^\epsilon(t))) (\mathbf{w}(\mathbf{x}) \\ & \quad + \mathbf{w}(\mathbf{y})) \cdot \mathbf{e}_{\mathbf{y}-\mathbf{x}} d\mathbf{y} d\mathbf{x}, \end{aligned} \tag{45}$$

and we can rewrite (45) in \mathbf{x} and ξ variables to get

$$\begin{aligned} & \epsilon^2 \int_{P_\delta(t)} \int_{\mathcal{H}_1(0)} D_e^{\epsilon|\xi|} \left[\epsilon|\xi| \partial_S \mathcal{W}^\epsilon(D_e^{\epsilon|\xi|} \mathbf{u}^\epsilon \cdot \mathbf{e}) \mathbf{w} \cdot \mathbf{e} \right] d\xi d\mathbf{x} \\ &= \epsilon^2 \int_{\mathcal{H}_1(0)} \int_{(P_\delta(t) - \epsilon\xi) \setminus P_\delta(t)} \partial_S \mathcal{W}^\epsilon(D_e^{\epsilon|\xi|} \mathbf{u}^\epsilon \cdot \mathbf{e}) (\mathbf{w}(\mathbf{x}) \\ & \quad + \mathbf{w}(\mathbf{x} + \epsilon\xi)) \cdot \mathbf{e} d\mathbf{x} d\xi. \end{aligned} \tag{46}$$

Lastly a straight forward manipulation in (46) delivers the product rule:

Author Proof

Product rule

$$\begin{aligned} & \epsilon^2 \int_{P_\delta(t)} \int_{\mathcal{H}_1(0)} D_e^{\epsilon|\xi|} \left[\epsilon|\xi| \partial_S \mathcal{W}^\epsilon(D_e^{\epsilon|\xi|} \mathbf{u}^\epsilon \cdot \mathbf{e}) \mathbf{w}(\mathbf{x}) \cdot \mathbf{e} \right] d\xi dx \\ & = -\epsilon^2 \int_{P_\delta(t)} \int_{\mathcal{H}_1(0)} 2\partial_S \mathcal{W}^\epsilon(D_e^{\epsilon|\xi|} \mathbf{u}^\epsilon \cdot \mathbf{e}) \mathbf{e} \cdot \mathbf{w}(\mathbf{x}) d\xi dx \quad (47) \\ & \quad - \epsilon^2 \int_{P_\delta(t)} \int_{\mathcal{H}_1(0)} \epsilon|\xi| \partial_S \mathcal{W}^\epsilon(D_e^{\epsilon|\xi|} \mathbf{u}^\epsilon \cdot \mathbf{e}) D_e^{\epsilon|\xi|} \mathbf{w} \cdot \mathbf{e} d\xi dx. \end{aligned}$$

We now recover (18) from (8). Multiplying both sides of (8) by $\dot{\mathbf{u}}^\epsilon$, integration over $P_\delta(t)$, and applying the product rule gives

$$\begin{aligned} & \int_{P_\delta(t)} \partial_t \frac{\rho|\dot{\mathbf{u}}^\epsilon|^2}{2} dx \\ & = \epsilon^2 \int_{P_\delta(t)} \int_{\mathcal{H}_1(0)} 2\partial_S \mathcal{W}^\epsilon(D_e^{\epsilon|\xi|} \mathbf{u}^\epsilon \cdot \mathbf{e}) \dot{\mathbf{u}}^\epsilon(\mathbf{x}) \cdot \mathbf{e} d\xi dx \\ & = -\epsilon^2 \int_{P_\delta(t)} \int_{\mathcal{H}_1(0)} D_e^{\epsilon|\xi|} \left[\epsilon|\xi| \partial_S \mathcal{W}^\epsilon(D_e^{\epsilon|\xi|} \mathbf{u}^\epsilon \cdot \mathbf{e}) \dot{\mathbf{u}}^\epsilon(\mathbf{x}) \cdot \mathbf{e} \right] d\xi dx \quad (48) \\ & \quad - \epsilon^2 \int_{P_\delta(t)} \int_{\mathcal{H}_1(0)} \epsilon|\xi| \partial_S \mathcal{W}^\epsilon(D_e^{\epsilon|\xi|} \mathbf{u}^\epsilon \cdot \mathbf{e}) D_e^{\epsilon|\xi|} \dot{\mathbf{u}}^\epsilon \cdot \mathbf{e} d\xi dx \end{aligned}$$

Define the stress work density

$$W^\epsilon(\mathbf{x}, t) = \epsilon^2 \int_{\mathcal{H}_1(0)} \epsilon|\xi| \mathcal{W}^\epsilon(D_e^{\epsilon|\xi|} \mathbf{u}^\epsilon \cdot \mathbf{e}) d\xi. \quad (49)$$

We observe that the change in stress work density with respect to time (stress power density) is given by

$$\dot{W}^\epsilon = \int_{\mathcal{H}_1(0)} \epsilon^3 |\xi| \partial_S \mathcal{W}^\epsilon(D_e^{\epsilon|\xi|} \mathbf{u}^\epsilon \cdot \mathbf{e}) D_e^{\epsilon|\xi|} \dot{\mathbf{u}}^\epsilon \cdot \mathbf{e} d\xi, \quad (50)$$

and (48) becomes

$$\begin{aligned} & \int_{P_\delta(t)} \dot{T}^\epsilon + \dot{W}^\epsilon dx \\ & = - \int_{P_\delta(t)} \int_{\mathcal{H}_1(0)} \epsilon^2 D_e^{\epsilon|\xi|} \left[\epsilon|\xi| \partial_S \mathcal{W}^\epsilon(D_e^{\epsilon|\xi|} \mathbf{u}^\epsilon \cdot \mathbf{e}) \dot{\mathbf{u}}^\epsilon \cdot \mathbf{e} \right] d\xi dx, \quad (51) \end{aligned}$$

where $\dot{T}^\epsilon = \partial_t(\rho|\dot{\mathbf{u}}^\epsilon|^2/2)$.

Proceeding as in Freund (1990) and Willis (1975) we find the change of internal energy of $P_\delta(t)$. We consider the region R given by the tube in space time swept out by $P_\delta(t)$ moving with constant velocity V^ϵ in the x_1 direction. Here we consider the time interval $t_1 < t < t_2$. We write

$$\begin{aligned} & \int_{t_1}^{t_2} \int_{P_\delta(t)} \partial_t(T^\epsilon + W^\epsilon) dx dt \\ & = \int_R \partial_t(T^\epsilon + W^\epsilon) dx dt \quad (52) \\ & = \int_{\partial R} (T^\epsilon + W^\epsilon) \frac{dt}{dv} dS, \end{aligned}$$

where we have applied the divergence theorem and $\frac{dt}{dv}$ is the direction cosine of the exterior normal to R in the time direction and dS is the element of surface area.

We will parameterize the surface area element on the sides of ∂R as $dS = \sqrt{1 + (V^\epsilon)^2} ds dt$ and on the sides

$$\frac{dt}{dv} = -\frac{V^\epsilon \mathbf{e}^1 \cdot \mathbf{n}}{\sqrt{1 + (V^\epsilon)^2}}$$

where \mathbf{n} is the outward directed unit normal to $\partial P_\delta(t)$. Applying this to (52) gives the identity

$$\begin{aligned} & \int_{t_1}^{t_2} \int_{P_\delta(t)} \partial_t(T^\epsilon + W^\epsilon) dx dt \\ & = - \int_{t_1}^{t_2} \int_{\partial P_\delta(t)} (T^\epsilon + W^\epsilon) \mathbf{e}^1 \cdot \mathbf{n} V^\epsilon ds dt \quad (53) \\ & \quad + \int_{P_\delta(t_2)} T^\epsilon + W^\epsilon dx - \int_{P_\delta(t_1)} T^\epsilon + W^\epsilon dx, \end{aligned}$$

where the last two integrals are on the top and bottom faces of R at $t = t_2$ and t_1 respectively. Now take $t_1 = t$ and $t_2 = t + \Delta t$ divide by Δt and send $\Delta t \rightarrow 0$ in (53) to get the identity

$$\begin{aligned} & \int_{P_\delta(t)} \partial_t(T^\epsilon + W^\epsilon) dx = \frac{d}{dt} \int_{P_\delta(t)} T^\epsilon + W^\epsilon dx \\ & \quad - \int_{\partial P_\delta(t)} (T^\epsilon + W^\epsilon) V^\epsilon \mathbf{e}^1 \cdot \mathbf{n} ds. \quad (54) \end{aligned}$$

This is equivalent to using Reynolds transport theorem but it is obtained in a way that **does not require** $\dot{\mathbf{u}}^\epsilon$ to be differentiable in space. So (54) together with (51) and (45) deliver the change in internal energy:

$$\begin{aligned} & \frac{d}{dt} \int_{P_\delta(t)} T^\epsilon + W^\epsilon dx \\ & = \int_{\partial P_\delta(t)} (T^\epsilon + W^\epsilon) V^\epsilon \mathbf{e}^1 \cdot \mathbf{n} ds \quad (55) \\ & \quad - \int_{A_\delta(t)} \int_{\mathcal{H}_\epsilon(\mathbf{x}) \cap P_\delta(t)} \partial_S \mathcal{W}^\epsilon(S(\mathbf{y}, \mathbf{x}, \mathbf{u}^\epsilon(t))) \mathbf{e}_{\mathbf{y}-\mathbf{x}} \\ & \quad \cdot (\dot{\mathbf{u}}^\epsilon(\mathbf{x}) + \dot{\mathbf{u}}^\epsilon(\mathbf{y})) d\mathbf{y} d\mathbf{x} \end{aligned}$$

and (18) follows.

7 Formulas for peridynamic stress work and convergence of peridynamic stress work and elastic energy flux to those of the local model

In this section we establish (23). We start by discovering the crucial identities (21) and (22). We denote the four sides of the rectangular contour Γ_δ by Γ_i , $i = 1, \dots, 4$ in Fig. 13. There is no contribution of the integrand to the integral on the lefthand side of (22) on

Author Proof

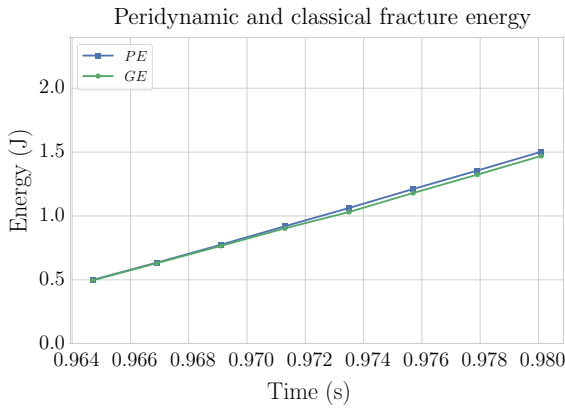


Fig. 12 Peridynamic and classical fracture energy. The interval along the y-axis is $[0, \mathcal{G}_c L]$, where L is the length of domain and is the maximum crack length

the sides 2 and 4 since $\mathbf{e}^1 \cdot \mathbf{n} = 0$ there. On side 3 the potential and kinetic energy densities are bounded so

$$\left| \int_{\Gamma_3} (T^\epsilon + W^\epsilon) V^\epsilon \mathbf{e}^1 \cdot \mathbf{n} ds \right| = O(\delta). \tag{56}$$

On side 1 we partition the contour Γ_1 into three parts. The first part is given by all points on Γ_1 that are further than ϵ away from $x_2 = 0$ call this $\Gamma_{1,+}$ and as before

$$\left| \int_{\Gamma_{1,+}} (T^\epsilon + W^\epsilon) V^\epsilon \mathbf{e}^1 \cdot \mathbf{n} ds \right| = O(\delta). \tag{57}$$

The part of Γ_1 with $0 \leq x_2 \leq \epsilon$ is denoted $\Gamma_{1,+}^+$ and the part with $-\epsilon \leq x_2 < 0$ is denoted $\Gamma_{1,+}^-$ and

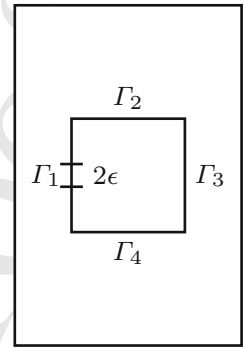
$$\left| \int_{\Gamma_{1,\pm}^+} T^\epsilon V^\epsilon \mathbf{e}^1 \cdot \mathbf{n} ds \right| = O(\delta). \tag{58}$$

Now we calculate

$$\begin{aligned} & \int_{\Gamma_{1,+}^+} W^\epsilon V^\epsilon \mathbf{e}^1 \cdot \mathbf{n} ds \\ &= -V^\epsilon \int_{\Gamma_{1,+}^+} W^\epsilon ds \\ &= -V^\epsilon \int_{\Gamma_{1,+}^+} \int_{\mathcal{H}_\epsilon(\mathbf{x}) \cap K_\epsilon^+} |\mathbf{y} - \mathbf{x}| \mathcal{W}^\epsilon(S(\mathbf{y}, \mathbf{x}, \mathbf{u}^\epsilon(t))) dy ds \\ &\quad - V^\epsilon \int_{\Gamma_{1,+}^+} \int_{\mathcal{H}_\epsilon(\mathbf{x}) \cap K_\epsilon^-} |\mathbf{y} - \mathbf{x}| \mathcal{W}^\epsilon(S(\mathbf{y}, \mathbf{x}, \mathbf{u}^\epsilon(t))) dy ds \end{aligned} \tag{59}$$

Here $\mathcal{H}_\epsilon(\mathbf{x}) \cap K_\epsilon^+$ is the subset of \mathbf{y} in $\mathcal{H}_\epsilon(\mathbf{x})$ for which the vector with end points \mathbf{y} and \mathbf{x} crosses the failure zone centerline and $\mathcal{H}_\epsilon(\mathbf{x}) \cap K_\epsilon^-$ is the subset of \mathbf{y} in $\mathcal{H}_\epsilon(\mathbf{x})$ for which the vector with end points \mathbf{y} and \mathbf{x} does not cross the failure zone centerline. Calculation

Fig. 13 The sides of the contour Γ_δ is denoted by Γ_1 through Γ_4



as in Sect. 3 gives

$$\begin{aligned} & \int_{\Gamma_1^+} \int_{\mathcal{H}_\epsilon(\mathbf{x}) \cap K_\epsilon^+} |\mathbf{y} - \mathbf{x}| \mathcal{W}^\epsilon(S(\mathbf{y}, \mathbf{x}, \mathbf{u}^\epsilon(t))) dy ds \\ &= \int_0^\epsilon \int_z^\epsilon \int_0^{\arccos(z/\zeta)} \mathcal{W}^\epsilon(S_+) \zeta^2 d\psi d\zeta dz \\ &= \frac{\mathcal{G}_c}{2}, \end{aligned} \tag{60}$$

and it follows from calculating as in (15) we get that

$$\left| \int_{\Gamma_1^+} \int_{\mathcal{H}_\epsilon(\mathbf{x}) \cap K_\epsilon^-} |\mathbf{y} - \mathbf{x}| \mathcal{W}^\epsilon(S(\mathbf{y}, \mathbf{x}, \mathbf{u}^{\epsilon n}(t))) dy ds \right| = O(\delta). \tag{61}$$

From (60) and (61) we conclude that

$$\begin{aligned} & \int_{\Gamma_1^+} W^\epsilon V^\epsilon \mathbf{e}^1 \cdot \mathbf{n} ds = -V^\epsilon \int_{\Gamma_1^+} W^\epsilon ds \\ &= -V^\epsilon \frac{\mathcal{G}_c}{2} + O(\delta). \end{aligned} \tag{62}$$

An identical calculation shows

$$\int_{\Gamma_1^-} W^\epsilon V^\epsilon \mathbf{e}^1 \cdot \mathbf{n} ds = -V^\epsilon \frac{\mathcal{G}_c}{2} + O(\delta). \tag{63}$$

and (21) and (22) follow.

To conclude we show

$$\lim_{\epsilon \rightarrow 0} E^\epsilon(\Gamma_\delta(t)) = - \int_{\Gamma_\delta} \mathbb{C} \mathcal{E} \mathbf{u}^0 \mathbf{n} \cdot \dot{\mathbf{u}}^0 ds. \tag{64}$$

Setting $\Delta_{\epsilon\xi} \dot{\mathbf{u}}^\epsilon(\mathbf{x}) = \dot{\mathbf{u}}^\epsilon(\mathbf{x}) + \dot{\mathbf{u}}^\epsilon(\mathbf{x} + \epsilon\xi)$ we have

$$\begin{aligned} & E^\epsilon(\Gamma_\delta(t)) \\ &= \epsilon^2 \int_{P_\delta(t)} \int_{\mathcal{H}_1(0)} D_e^{\epsilon|\xi|} \\ & \quad \left[\epsilon |\xi| \partial_S \mathcal{W}^\epsilon(D_e^{\epsilon|\xi|} \mathbf{u}^\epsilon \cdot \mathbf{e}) \dot{\mathbf{u}}^\epsilon \cdot \mathbf{e} \right] d\xi dx \\ &= \epsilon^2 \int_{\mathcal{H}_1(0)} \int_{(P_\delta(t) - \epsilon\xi) \setminus P_\delta(t)} \partial_S \mathcal{W}^\epsilon(D_e^{\epsilon|\xi|} \mathbf{u}^\epsilon \cdot \mathbf{e}) \\ & \quad \Delta_{\epsilon\xi} \dot{\mathbf{u}}^\epsilon(\mathbf{x}) \cdot \mathbf{e} dx d\xi. \end{aligned} \tag{65}$$

Integration in the ξ variable is over the unit disc centered at the origin $\mathcal{H}_1(0)$. We split the unit disk into its four quadrants $Q_i, i = 1, \dots, 4$. The boundary Γ_δ is the union of its four sides $\Gamma_j, j = 1, \dots, 4$. Here the left and right sides are Γ_1 and Γ_3 respectively and the top and bottom sides are Γ_2 and Γ_4 respectively, see Fig. 14. We choose \mathbf{n} to be the outward pointing normal vector to P_δ , \mathbf{t} is the tangent vector to the boundary Γ_δ and points in the clockwise direction, and $\mathbf{e} = \xi/|\xi|$. For ξ in Q_1 the set of points $\mathbf{x} \in (P_\delta(t) - \epsilon\xi) \setminus P_\delta(t)$ is parameterized as $\mathbf{x} = \mathbf{t}x + \mathbf{n}(\epsilon|\xi|\mathbf{e} \cdot \mathbf{n})r$. Here x lies on $\Gamma_1 \cup \Gamma_4$ and $0 < r < 1$ and the area element is $-\epsilon|\xi|\mathbf{e} \cdot \mathbf{n} dx dr$. For ξ in Q_2 the set of points $\mathbf{x} \in (P_\delta(t) - \epsilon\xi) \setminus P_\delta(t)$ is again parameterized as $\mathbf{x} = \mathbf{t}x + \mathbf{n}(\epsilon|\xi|\mathbf{e} \cdot \mathbf{n})r$ where x lies on $\Gamma_3 \cup \Gamma_4$ and $0 < r < 1$ and the area element is given by the same formula. For ξ in Q_3 we have the same formula for the area element and parameterization and x lies on $\Gamma_3 \cup \Gamma_4$ with $0 < r < 1$. Finally for ξ in Q_4 we have again the same formula for the area element and parameterization and x lies on $\Gamma_1 \cup \Gamma_2$ with $0 < r < 1$. This parameterization and a change in order of integration delivers the formula for $E^\epsilon(\Gamma_\delta(t))$ given by

$$\begin{aligned}
 E^\epsilon(\Gamma_\delta(t)) &= - \int_{\Gamma_1} \int_0^1 \int_{\mathcal{H}_1(0) \cap (Q_1 \cup Q_4)} \epsilon^3 |\xi| \partial_S \mathcal{W}^\epsilon(D_e^{\epsilon|\xi|} \mathbf{u}^\epsilon \cdot \mathbf{e}) \\
 &\quad \Delta_{\epsilon\xi} \dot{\mathbf{u}}^\epsilon(\mathbf{x}) \cdot \mathbf{e} \mathbf{n} \cdot \mathbf{e} d\xi dr dx \\
 &\quad - \int_{\Gamma_2} \int_0^1 \int_{\mathcal{H}_1(0) \cap (Q_3 \cup Q_4)} \epsilon^3 |\xi| \partial_S \mathcal{W}^\epsilon(D_e^{\epsilon|\xi|} \mathbf{u}^\epsilon \cdot \mathbf{e}) \\
 &\quad \Delta_{\epsilon\xi} \dot{\mathbf{u}}^\epsilon(\mathbf{x}) \cdot \mathbf{e} \mathbf{n} \cdot \mathbf{e} d\xi dr dx \\
 &\quad - \int_{\Gamma_3} \int_0^1 \int_{\mathcal{H}_1(0) \cap (Q_2 \cup Q_3)} \epsilon^3 |\xi| \partial_S \mathcal{W}^\epsilon(D_e^{\epsilon|\xi|} \mathbf{u}^\epsilon \cdot \mathbf{e}) \\
 &\quad \Delta_{\epsilon\xi} \dot{\mathbf{u}}^\epsilon(\mathbf{x}) \cdot \mathbf{e} \mathbf{n} \cdot \mathbf{e} d\xi dr dx \\
 &\quad - \int_{\Gamma_4} \int_0^1 \int_{\mathcal{H}_1(0) \cap (Q_1 \cup Q_2)} \epsilon^3 |\xi| \partial_S \mathcal{W}^\epsilon(D_e^{\epsilon|\xi|} \mathbf{u}^\epsilon \cdot \mathbf{e}) \\
 &\quad \Delta_{\epsilon\xi} \dot{\mathbf{u}}^\epsilon(\mathbf{x}) \cdot \mathbf{e} \mathbf{n} \cdot \mathbf{e} d\xi dr dx \\
 &\quad + O(\epsilon).
 \end{aligned} \tag{66}$$

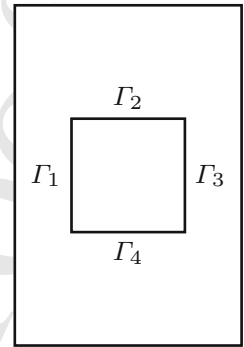
When $\mathbf{u}^\epsilon \rightarrow \mathbf{u}^0$ one applies Taylor series to each integrand and passes to the $\epsilon = 0$ limit to get that each integrand in the limit is given by

$$\frac{4|\xi|}{\omega_2} J(|\xi|) h'(0) \mathcal{E} \mathbf{u}^0 \mathbf{e} \cdot \mathbf{e} (\dot{\mathbf{u}}^0 \cdot \mathbf{e}) (\mathbf{n} \cdot \mathbf{e}) \tag{67}$$

so

$$\begin{aligned}
 \lim_{\epsilon \rightarrow 0} E^\epsilon(\Gamma_\delta(t)) &= - \frac{1}{\omega_2} \int_{\Gamma_1} \int_0^1 \int_{\mathcal{H}_1(0) \cap (Q_1 \cup Q_4)} 4|\xi| J(|\xi|) h'(0) \mathcal{E} \mathbf{u}^0 \mathbf{e} \\
 &\quad \cdot \mathbf{e} (\dot{\mathbf{u}}^0 \cdot \mathbf{e}) (\mathbf{n} \cdot \mathbf{e}) d\xi dr dx
 \end{aligned}$$

Fig. 14 Contour Γ_δ split into four sides



$$\begin{aligned}
 &- \frac{1}{\omega_2} \int_{\Gamma_2} \int_0^1 \int_{\mathcal{H}_1(0) \cap (Q_3 \cup Q_4)} 4|\xi| J(|\xi|) h'(0) \mathcal{E} \mathbf{u}^0 \mathbf{e} \\
 &\quad \cdot \mathbf{e} (\dot{\mathbf{u}}^0 \cdot \mathbf{e}) (\mathbf{n} \cdot \mathbf{e}) d\xi dr dx \\
 &- \frac{1}{\omega_2} \int_{\Gamma_3} \int_0^1 \int_{\mathcal{H}_1(0) \cap (Q_2 \cup Q_3)} 4|\xi| J(|\xi|) h'(0) \mathcal{E} \mathbf{u}^0 \mathbf{e} \\
 &\quad \cdot \mathbf{e} (\dot{\mathbf{u}}^0 \cdot \mathbf{e}) (\mathbf{n} \cdot \mathbf{e}) d\xi dr dx \\
 &- \frac{1}{\omega_2} \int_{\Gamma_4} \int_0^1 \int_{\mathcal{H}_1(0) \cap (Q_1 \cup Q_2)} 4|\xi| J(|\xi|) h'(0) \mathcal{E} \mathbf{u}^0 \mathbf{e} \\
 &\quad \cdot \mathbf{e} (\dot{\mathbf{u}}^0 \cdot \mathbf{e}) (\mathbf{n} \cdot \mathbf{e}) d\xi dr dx.
 \end{aligned} \tag{68}$$

Noting that the integrand has radial symmetry in the ξ variable and (15) (see the calculation below Lemma 6.6 of Lipton (2016)) one obtains

$$\lim_{\epsilon \rightarrow 0} E^\epsilon(\Gamma_\delta(t)) = - \sum_{i=1}^4 \frac{1}{2} \int_{\Gamma_i} 2\mathbb{C} \mathcal{E} \mathbf{u}^0 \mathbf{n} \cdot \dot{\mathbf{u}}^0 dx, \tag{69}$$

and (64) follows.

Identical calculations give (37) when we use the contour S_δ and compute the change in energy internal to Q_δ in Fig. 7.

8 Conclusions

It has been shown for the nonlocal model that that the net flux of stress work density through a small contour surrounding the crack is the power per unit length needed to create new fracture surface. This is derived directly from Cauchy's equations of motion for a continuum body (8) (see Sect. 4). In this paper the power balance and kinetic relation given by (27), (28) is not postulated but instead recovered directly from (18) by taking the $\epsilon = 0$ limit. For this case the generalized Irwin relationship is shown to be a consequence of the cohesive dynamics in the $\epsilon = 0$ limit. The recovery is possible since the nonlocal model is well defined

770 over the failure zone. This suggests that the double well
 771 potential of cohesive dynamics provides a phenomeno-
 772 logical description of the process zone at mesoscopic
 773 length scales. We have illustrated the ideas using the
 774 simplest double well energy for a bond based peridy-
 775 namic formulation. Future investigations will consider
 776 state based peridynamic models.

777 Last we mention that if one fixes the horizon then
 778 the ratio r_c to r^+ will affect the size of the process
 779 zone hence a brittle to quasi brittle behavior can be
 780 expected depending on the ratio. On the other hand for
 781 any fixed ratio of r_c to r^+ the process zone goes to
 782 zero as the horizon goes to zero and we recover brittle
 783 fracture, this is shown theoretically in Lipton (2016). In
 784 addition the fracture toughness for the nonlocal model
 785 depends on the area underneath the force strain curve
 786 and is insensitive to the ratio. This is why this ratio does
 787 not show up in the calculations associated with $\epsilon \rightarrow 0$.

788 **References**

789 Atkinson C, Eshelby JD (1968) The flow of energy into the tip
 790 of a moving crack. *Int J Fract* 4:3–8
 791 Anderson TL (2005) *Fracture mechanics: fundamentals and*
 792 *applications*, 3rd edn. Taylor & Francis, Boca Raton
 793 Bouchbinder E, Goldman T, Fineberg J (2014) The dynamics of
 794 rapid fracture: instabilities, nonlinearities and length scales.
 795 *Rep Prog Phys* 77(4):046501
 796 Freund LB (1972) Energy flux into the tip of an extending crack
 797 in an elastic solid. *J Elast* 2:341–349
 798 Freund B (1990) *Dynamic fracture mechanics*. Cambridge
 799 *Monographs on Mechanics and Applied Mathematics*.
 800 Cambridge University Press, Cambridge
 801 Freund B, Clifton RJ (1974) On the uniqueness of plane elasto-
 802 dynamic solutions for running cracks. *J Elast* 4:293–299
 803 Goldman T, Livne A, Fineberg J (2010) Acquisition of inertia by
 804 a moving crack. *Phys Rev Lett* 104(11):114301
 805 Ha YD, Bobaru F (2010) Studies of dynamic crack propaga-
 806 tion and crack branching with peridynamics. *Int J Fract*
 807 162:229–244
 808 Hu W, Ha YD, Bobaru F, Silling S (2012) The formulation and
 809 computation of the nonlocal J-integral in bond-based peri-
 810 dynamics. *Int J Fract* 176:195–206
 811 Irwin G R (1967) Constant speed, semi-infinite tensile crack
 812 opened by a line force. *Lehigh University Memorandum*
 813 Jha PK, Lipton, (2020) Finite element convergence for state-
 814 based peridynamic fracture models. *Commun Appl Math*
 815 *Comput* 2:93–128
 816 Jha PK, Lipton R (2019b) Numerical convergence of finite dif-
 817 ference approximations for state based peridynamic frac-

818 ture models. *Comput Meth Appl Mech Eng* 351:184–225. 818
<https://doi.org/10.1016/j.cma.2019.03.024> 819
 Kostrov BV, Nikitin LV (1970) Some general problems of 820
 mechanics of brittle fracture. *Arch Mech Stosowanej.* 821
 22:749–775 822
 Lipton R (2014) Dynamic brittle fracture as a small horizon limit 823
 of peridynamics. *J Elast* 117(1):21–50 824
 Lipton R (2016) Cohesive dynamics and brittle fracture. *J Elast* 825
 124(2):143–191 826
 Lipton R, Jha P K (2020). Plane elastodynamic solutions for run- 827
 ning cracks as the limit of double well nonlocal dynamics. 828
[arXiv:2001.00313](https://arxiv.org/abs/2001.00313) 829
 Mott NF (1948) Fracture in mild steel plates. *Engineering* 830
 165:16–18 831
 Nillison F (1974) A note on the stress singularity at a non- 832
 uniformly moving crack tip. *J Elast* 4:293–299 833
 Ravi-Chandar K (2004) *Dynamic fracture*. Elsevier, Oxford 834
 Rice JR (1968) A path independent integral and the approximate 835
 analysis of strain concentration by notches and cracks. *J* 836
Appl Mech 9:379–386 837
 Rice JR (1968) *Mathematical analysis in the mechanics of frac-* 838
ture. Fracture: An advanced treatise, vol II. Academic Press, 839
 New York, p 191 840
 Stenström C, Eriksson K (2019) The J-contour integral in peri- 841
 dynamics via displacements. *Int J Fract* 216:173–183 842
 Sih GC (1968) Some elastodynamic problems of cracks. *Int J* 843
Fract Mech 4:51–68 844
 Sih GC (1970) Dynamic aspects of crack propagation. *Inelastic* 845
Behavior of Solids, McGraw-Hill, pp 607–633 846
 Silling SA (2000) Reformulation of elasticity theory for dis- 847
 continuities and long-range forces. *J Mech Phys Solids* 848
 48(1):175–209 849
 Silling SA, Epton M, Weckner O, Xu J, Askari E (2007) Peridy- 850
 namic states and constitutive modeling. *J Elast* 88(2):151– 851
 184 852
 Silling SA, Lehoucq RB (2010) Peridynamic theory of solid 853
 mechanics. *Adv Appl Mech* 44:73–168 854
 S. A. and Askari, E., (2005) A meshfree method based on 855
 the peridynamic model of solid mechanics. *Comput Struct* 856
 83:1526–1535 857
 Slepian Y (2002) *Models and phenomena in fracture mechanics* 858
foundations of engineering mechanics. Springer, Berlin 859
 Willis JR (1975) *Equations of motion for propagating cracks.* 860
The mechanics and physics of fracture. The Metals Society, 861
 New York, pp 57–67 862

Publisher's Note Springer Nature remains neutral with regard 863
 to jurisdictional claims in published maps and institutional affil- 864
 iations. 865

Journal: 10704
Article: 480

Author Query Form

**Please ensure you fill out your response to the queries raised below
and return this form along with your corrections**

Dear Author

During the process of typesetting your article, the following queries have arisen. Please check your typeset proof carefully against the queries listed below and mark the necessary changes either directly on the proof/online grid or in the 'Author's response' area provided below

Query	Details required	Author's response
1.	Affiliations: Journal instruction requires a country for affiliations; however, this is missing in affiliations 1 and 2. Please verify if the provided country is correct and amend if necessary.	